WEP Warwick Evans Publishing

International Journal of Materials Science and Technology Studies

ISSN: 3006-7693 (Print), ISSN: 3006-3744 (Online) | Volume 3, Number 2, Year 2025
DOI: https://doi.org/10.62051/ijmsts.v3n2.04
Journal homepage: https://wepub.org/index.php/IJMSTS/index

The Effect of Hydrothermal Aging on the Non-Isothermal Crystallization Behavior of Polyamide 6

Xinyang Zhang

School of Material Science and Engineering, Henan Polytechnic University, Jiaozuo, 454000, China

ABSTRACT

Polyamide 6 (PA6) is an important semi-crystalline engineering plastic widely used in electrical appliances, automotive materials, and other applications. However, PA6 is highly susceptible to moisture absorption, which can significantly alter its physicochemical properties. In this study, PA6 was synthesized via anionic ring-opening polymerization, and immersion tests were conducted in accordance with ISO 175:2010. The influence of environmental factors on the non-isothermal crystallization behavior of PA6 was investigated. The Mo equation was successfully employed to characterize the entire non-isothermal crystallization process. The obtained kinetic parameters provide valuable insights for predicting the performance of PA6 under practical conditions and serve as a reference for the modification and optimization of PA6.

KEYWORDS

Environmental effects; Immersion test; Polyamide 6; Mo equation; Non-isothermal crystallization kinetics

1. INTRODUCTION

Polyamide 6 (PA6) is a significant semi-crystalline engineering plastic that can even replace steel in some applications [1-5]. However, PA6 is highly moisture sensitive, and compared to steel, its properties are significantly affected by changes in environmental conditions [6, 7]. Over the past few decades, polyamide materials have also been used in harsh environments characterized by high strength, high temperatures, and high relative humidity. Polyamide materials used in construction machinery are often exposed to complex and variable environmental conditions, such as exposure to water and fuel [8, 10]. Therefore, detailed studies of the effects of these two fluids on PA6's structural properties are necessary.

As we all know, the amide group in the PA6 molecular chain is prone to forming hydrogen bonds with water molecules, resulting in a high water absorption rate [11, 12]. The molecular chains bound to water are more likely to slide under external loads, decreasing the stiffness and strength of PA6 while significantly increasing its toughness [6, 13-15]. This phenomenon is known as water plasticization, and the effect of water plasticization on polyamide materials has been discussed in previous articles. Manker et al. [16] studied polyamide-based polymers' mechanical and dynamic mechanical properties under three conditions: dry, at equilibrium at 50% relative humidity, and fully water-saturated. The results showed that moisture significantly decreased the samples' mechanical strength and glass transition temperature. Some articles have also reported the effects of water plasticization on polyamides, including the weakening of intermolecular forces, a decrease in dimensional stability, and a decrease in modulus [17-20].

During the oil immersion process, oil molecules penetrate the sample, and unreacted monomers and oligomers migrate into the oil, depending on the oil's polarity and temperature [21-24]. Bawase M et al. [25] immersed PA66 in a mixture of methanol and gasoline and observed changes in the weight and tensile strength of the PA66 sample. Furthermore, they confirmed the precipitation of monomers into the oil by FT-IR analysis. Bernardo et al. [26] also reported mass loss and property changes of PA6 immersed in a lubricant matrix. Several studies have reported similar mass and property changes in polyamide materials immersed in organic solutions, which are influenced by temperature and fluid type [27, 28]. In addition, some articles mention a decrease in the mechanical properties and an increase in the tribological properties of polyamide after oil immersion [29, 30].

However, most articles have almost exclusively focused on the influence of environmental factors on the mechanical properties, tribological properties, and hardness of PA6. In contrast, there have been relatively few studies on the impact of environmental factors on the crystallization behavior of PA6. As we all know, crystallization behavior affects crystalline polymers' properties. In this study, PA6 immersion experiments were carried out using IRM 903 standard oil and pure water according to ISO 175: 2010. The compatibility of PA6 with water and fuel was evaluated, and the previous part of the study was compared using non-isothermal crystallization kinetic analysis. This study aimed to explore the actual service performance of PA6 by revealing the changes caused by liquid exposure.

2. EXPERIMENT

2.1. Materials

The ε-caprolactam (CL) and sodium hydroxide (NaOH) utilized in this study were procured from the China Petroleum & Chemical Corporation (Sinopec). Shanghai McLean Biochemical Technology Co., Ltd., China, synthesized the toluene diisocyanate (TDI).

2.2. Methods

In this study, an immersion test was used to investigate the compatibility of PA6 with moisture and standard oil. The samples were processed from caprolactam polymerized sheets. The immersion test was carried out in a beaker and maintained at the specified temperature for 168 hours (one week). The heating process was carried out in an oil bath. These tests are based on the methods outlined in ISO 175:2010 and carried out at 23°C and 70°C, respectively. For convenience, the samples immersed in standard oil at 70℃ and 23℃ are named PA6-70O and PA6-23O, respectively. The samples stored in the air are PA6-air-cured. The samples immersed in water at 70℃ and 23℃ are PA6-70W and PA6-23W, respectively.

2.3. Synthesis of PA6

Polyamide 6 (PA6) is synthesized in a three-necked glass reactor with a round bottom. Initially, ε-caprolactam (CL) is melted under a vacuum of -0.1 MPa for 40 minutes to remove moisture. Sodium hydroxide (NaOH) is then introduced into the system and maintained at 140°C for 30 minutes. Finally, the activator TDI is introduced, and the final mixture is immediately transferred to a preheated reactor in an oven at 160°C, where it polymerizes for 120 minutes.

2.4. Non-Isothermal Crystallization Kinetics Analysis

The non-isothermal crystallization kinetics of the studied samples were studied using a DSC3 analyzer (Mettler Toledo, Switzerland). Each sample was initially heated from 23℃ to 250℃ at 10℃/min. It was then held at 250℃ for 5 minutes to eliminate thermal history. Afterwards, the sample was cooled to 50℃ at different cooling rates (φ) of 15, 20, 25, and 30 ℃/min.

3. RESULTS AND DISCUSSION

3.1. Non-Isothermal Crystallization Behavior of PA6

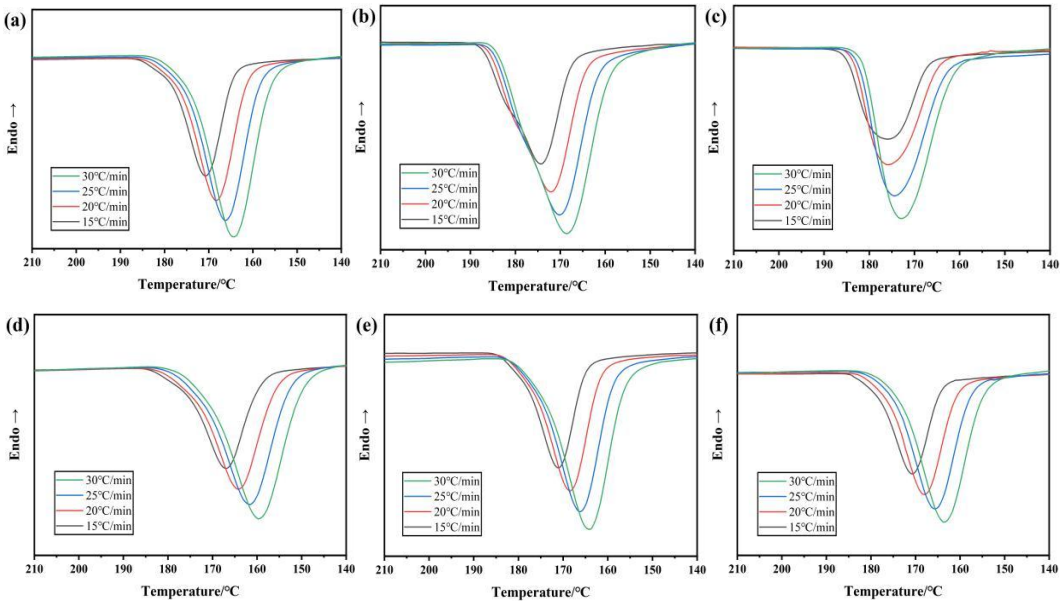

Figure 1. Non-isothermal melt-crystallization exotherm at different cooling rates: (a) PA6, (b) PA6-70O, (c) PA6-70W, (d) PA6-air-cured, (e) PA6-23W, (f) PA6-23O

Table 1. Crystallization kinetic behavior parameters

Sample	Φ(℃/min)	T_o(℃)	T_p(℃)	ΔH_c(J/g)	$t_{1/2}$(min)
PA6	15	187.03	170.80	68.99	5.08
	20	186.70	168.49	71.81	3.85
	25	185.46	166.19	70.95	3.11
	30	184.55	164.20	72.99	2.61
PA6 immersed in standard oil (70℃)	15	191.50	174.25	102.59	4.95
	20	190.00	172.00	94.19	3.74
	25	187.92	170.42	90.65	3.01
	30	187.00	168.50	93.38	2.46
PA6 immersed in water (70℃)	15	192.08	175.75	104.77	3.43
	20	188.5	175.67	96.32	2.58
	25	187.72	174.58	90.19	2.08
	30	186.67	172.50	94.90	1.73
PA6 air-cured	15	186.54	168.83	69.74	3.88
	20	184.72	164.36	69.33	2.96
	25	183.81	161.72	65.78	2.46
	30	182.57	159.74	67.09	2.05
PA6 immersed in water (23℃)	15	186.06	170.63	72.95	3.60
	20	184.73	168.16	67.80	2.76
	25	184.24	166.02	66.85	2.32
	30	183.09	164.22	67.81	1.91
PA6 immersed in standard oil (23℃)	15	185.73	170.51	93.31	3.68
	20	184.07	167.72	88.22	2.85
	25	183.07	165.75	86.29	2.34
	30	182.60	163.72	85.74	1.98

Figure 1 shows the crystalline heat release diagram of the studied samples at four different cooling rates (φ): 15, 20, 25, and 30 ℃/min. Table 1 presents the functional kinetic parameters derived from these curves. They include the onset temperature of the crystallization (T_o), the temperature of the exothermic peak (T_p), the crystallization enthalpy (ΔH_c), and the crystallization half-time ($t_{1/2}$).

It can be seen from these curves that the crystallization peaks of PA6 were single-peaked [9, 15]. As the cooling rate increases, the T_p peak value increases and shifts to lower temperatures. The T_p, T_o, and ΔH_c of the samples immersed at 70℃ were higher than those of the original PA6 at all cooling rates, indicating enhanced crystallization. This means that annealing and recrystallization promote the crystallization behavior of PA6. However, the changes in crystallization behavior were relatively minor for samples immersed in water at 23℃ and those stored in the air. In contrast, samples immersed in 23℃ standard oil showed a significant increase in crystallization enthalpy, which can be attributed to the specific effects of IRM 903 standard oil on PA6 [26].

Integrating the non-isothermal crystallization exothermic peaks for all PA6 samples using Equation 1, we obtained relative crystallinity profiles as a function of temperature.

$$X_t = \frac{\int_{T_0}^{T} \frac{dH_c/dt}{dT/dt} dT}{\int_{T_0}^{T_d} \frac{dH_c/dt}{dT/dt} dT} \times 100\% \quad (1)$$

Where T_0 and T_d indicate the initial crystallization temperature and the end crystallization temperature, T represents the crystallization temperature at the time t, and H_c represents the total crystallization enthalpy at the crystallization time t.

In non-isothermal crystallization, the temperature (T) can be transformed into the crystallization time (t) using Equation 2:

$$t = (T_0 - T)/\Phi \quad (2)$$

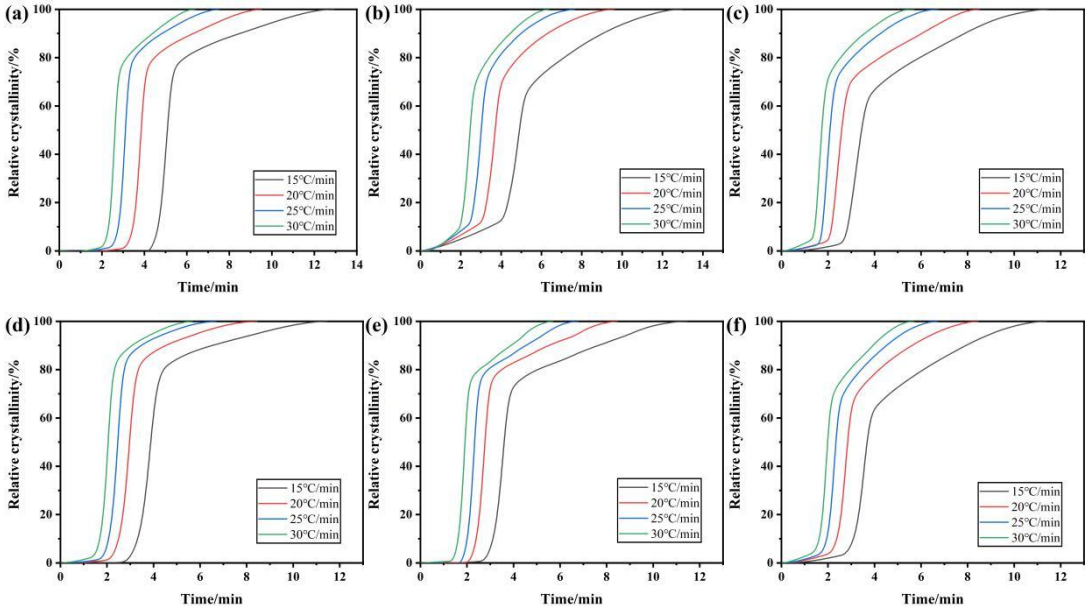

Figure 2. The relative crystallinity, X_t, at the various crystallization temperatures in the process of non-isothermal crystallization: (a) PA6, (b) PA6-70O, (c) PA6-70W, (d) PA6-air-cured, (e) PA6-23W, (f) PA6-23O

Where T is the temperature at crystallization time and φ denotes the cooling rate. The value of T on the X-axial can be transformed into t, as shown in Figure 2.

All curves are S-shaped with two non-linear stages. The early phase (first non-linear stage) corresponds to rapid primary crystallization due to nucleation. In contrast, the late phase (second non-linear stage) is characterized by slow secondary crystallization due to the impact of crystallizing spheres. Additionally, as the cooling rates increase, all the curves shift to the left along the X-axis, indicating a faster crystallization rate with higher cooling rates. Notably, the $t_{1/2}$ values of the immersed samples and those stored in the air were lower than those of the original PA6. This decrease may be attributed to the interaction of the fluid with the polymer molecular chains, which lowers the glass transition temperature and thus promotes easier crystallization [10, 13, 17, 26].

3.2. Non-isothermal Crystallization Kinetics of PA6

Since the degree of crystallinity is influenced by both the φ and the t, for the specified degree of crystallinities (20%, 40%, 60%, 80%), the Mo equation can be used to generate a fitting plot with the $lg\Phi$ as the y-axis and the lgt as the x-axis. This approach provides insight into the kinetics and transformation mechanisms of the crystallization process:

$$lg\Phi = lgF(T) - \alpha lgt \tag{3}$$

$$\alpha = \frac{n}{m} \tag{4}$$

Here, F(T) represents the cooling rate required for the system to achieve a certain relative degree of crystallization per unit of time. The parameter α is the ratio between Avrami (n) and Ozawa (m) exponents. The values of α and F(T) can be determined from the fitting curves' slope and the intercept with the y-axis, respectively. The results are presented in Table 2. Figure 3 presents the plots of $lg\varphi$ versus lgt at various degree crystallinities for the studied PA6 samples. The figures show good linearity, verifying that the Mo method correctly describes the systems' non-isothermal crystallization kinetics.

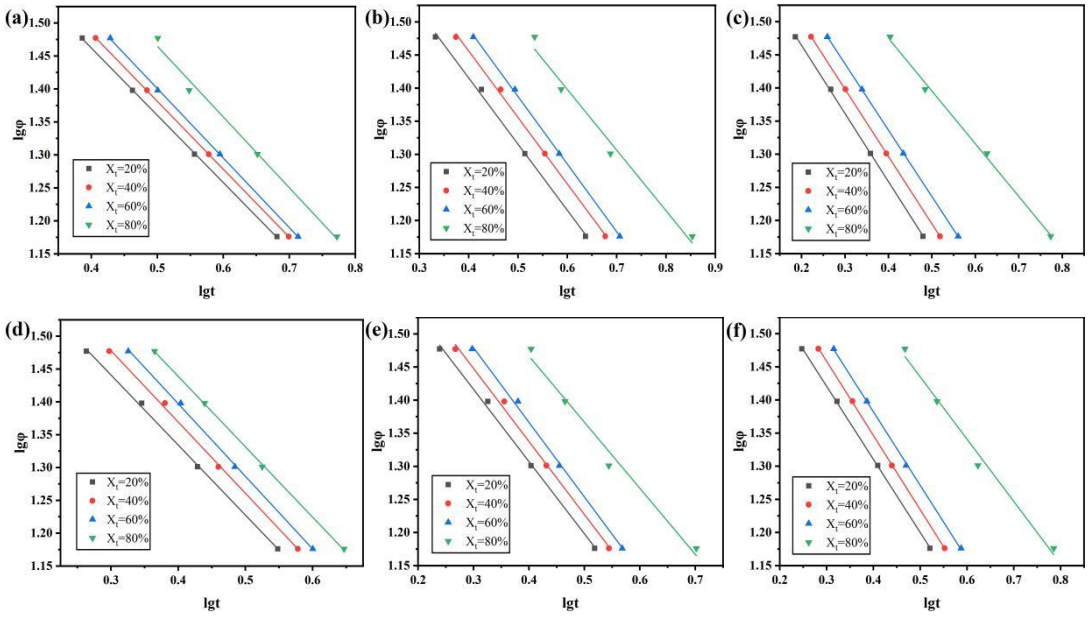

Figure 3. Plots of log φ versus log t at different crystallinity: (a) PA6, (b) PA6-70O, (c) PA6-70W, (d) PA6-air-cured, (e) PA6-23W, (f) PA6-23O.

The higher the sample's F(T) and α values, the more difficult it is to crystallize. At the same degree of crystallinity, the α value of all PA6 samples is close to 1. It is worth noting that for a given crystallinity (20%, 40%, 60%, 80%), the F(T) values of the samples after the immersion experiment were lower than those of the original PA6 samples. The samples immersed in standard oil and water

at 70℃ showed the lowest and highest F(T) reduction, respectively, while the other three groups of samples had similar values. These findings are consistent with the previous observations.

Table 2. Non-isothermal crystallization kinetics parameters for the studied samples at various relative crystallinity by the Mo equation.

X_t/%	PA6		PA6-70O		PA6-70W		PA6-air-cured		PA6-23W		PA6-23O	
	α	F(T)	A	F(T)	α	F(T)	α	F(T)	α	F(T)	α	F(T)
20	1.02	74.13	0.99	66.07	1.02	46.77	1.06	57.54	1.09	54.95	1.10	56.23
40	1.03	79.43	1.00	72.44	1.01	50.12	1.08	60.10	1.10	60.26	1.11	61.66
60	1.05	85.11	1.02	79.43	1.00	54.95	1.10	68.18	1.12	66.10	1.11	67.61
80	1.07	100.00	0.91	89.13	0.79	61.66	1.07	74.13	0.99	74.13	0.94	79.43

4. CONCLUSION

In this study, PA6 was synthesized via anionic ring-opening polymerization. The effects of moisture and IRM 903 reference oil on the non-isothermal crystallization behavior of PA6 were investigated through immersion experiments. By revealing the changes induced by liquid exposure, the study aimed to explore the compatibility of PA6 with moisture and IRM 903 reference oil. Non-isothermal crystallization kinetics were analyzed using the Mo equation, and the results demonstrated that wet and thermal treatments reduced the intermolecular forces of PA6. Water interacts with the molecular chains of PA6 through hydrogen bonding, which weakens the intermolecular forces and enhances the mobility of the molecular chains. Consequently, this phenomenon manifests as a reduction in the crystallinity of the samples. In comparison to water, the influence of fuel on the crystallization behavior of PA6 was less pronounced.

DECLARATION OF CONFLICTING INTERESTS

There are no potential conflicts of interest concerning this article's research, authorship, and publication.

ACKNOWLEDGEMENTS

This research received no specific grant from any funding agency in the public, commercial, or not-for-profit sectors.

REFERENCES

[1] Li M, Qiu J, Yue Y, et al. The Preparation of Monomer Casting Polyamide 6/Thermotropic Liquid Crystalline Polymer Composite Materials with Satisfactory Miscibility. Polymers 2022; 14. DOI: 10.3390/polym14204355.

[2] Álvarez-Láinez ML and Palacio R JA. Correlations between thermal and tensile behavior with friction coefficient in copolyamides 6/12. Wear 2017; 372-373: 76-80. DOI: 10.1016/j.wear.2016.11.018.

[3] Zhang H-X, Park J-Y, Lee D-E, et al. Fabrication of PA6/MoS2 nanocomposites via melt blending of PA6 with PA6/PEG modified-MoS2 masterbatch. Polymer Bulletin 2022; 79: 10639-10652. DOI: 10.1007/s00289-021-04068-z.

[4] Yin X, Zhao X and Ye L. In situ-induced epiphytic crystallization of MC PA6 by self-assembled nucleator and reinforcing effect. Polymer International 2023; 72: 629-639. DOI: 10.1002/pi.6513.

[5] Skorupska M, Kulczyk M, Denis P, et al. Structural Hierarchy of PA6 Macromolecules after Hydrostatic Extrusion. Materials 2023; 16. DOI: 10.3390/ma16093435.

[6] Unnikrishnan V, Zabihi O, Li Q, et al. Multifunctional PA6 composites using waste glass fiber and green metal organic framework/graphene hybrids. Polymer Composites 2022; 43: 5877-5893. DOI: 10.1002/pc.27002.

[7] Liu H, Wang Z, Pan B, et al. Carbon felt/nitrogen-doped graphene/paraffin wax 3D skeleton regulated tribological performances of the MCPA6 composites: A novel strategy of oil embedding and transporting. Tribology International 2023; 184. DOI: 10.1016/j.triboint.2023.108440.

[8] Unal H and Mimaroglu A. Friction and wear performance of polyamide 6 and graphite and wax polyamide 6 composites under dry sliding conditions. Wear 2012; 289: 132-137. DOI: 10.1016/j.wear.2012.04.004.

[9] Rwei S-P, Ranganathan P, Chiang W-Y, et al. Synthesis of Low Melting Temperature Aliphatic-Aromatic Copolyamides Derived from Novel Bio-Based Semi Aromatic Monomer. Polymers 2018; 10. DOI: 10.3390/polym10070793.

[10] Hirai T, Onochi Y and Kawada J. Multifaceted property tailoring of polyamide 6 by blending miscible and immiscible components: ternary blends of polyamide 6/polyethylene terephthalate/phenol novolac. RSC Advances 2020; 10: 15132-15138. DOI: 10.1039/d0ra02344b.

[11] Carrascal I, Casado JA, Polanco JA, et al. Absorption and diffusion of humidity in fiberglass-reinforced polyamide. Polymer Composites 2005; 26: 580-586. DOI: 10.1002/pc.20134.

[12] Sun D, Li J, Pan Q, et al. The In Situ Polymerization and Characterization of PA6/LiCl Composites. Journal of Spectroscopy 2013; 2013: 1-4. DOI: 10.1155/2013/164275.

[13] Sambale AK, Stanko M, Emde J, et al. Characterisation and FE Modelling of the Sorption and Swelling Behaviour of Polyamide 6 in Water. Polymers 2021; 13. DOI: 10.3390/polym13091480.

[14] Oh K, Kim H and Seo Y. Effect of Diamine Addition on Structural Features and Physical Properties of Polyamide 6 Synthesized by Anionic Ring-Opening Polymerization of ε-Caprolactam. ACS Omega 2019; 4: 17117-17124. DOI: 10.1021/acsomega.9b01342.

[15] Lin H-M, Behera K, Yadav M, et al. Polyamide 6/Poly(vinylidene fluoride) Blend-Based Nanocomposites with Enhanced Rigidity: Selective Localization of Carbon Nanotube and Organoclay. Polymers 2020; 12. DOI: 10.3390/polym12010184.

[16] Manker LP, Hedou MA, Broggi C, et al. Performance polyamides built on a sustainable carbohydrate core. Nature Sustainability 2024; 7: 640-651. DOI: 10.1038/s41893-024-01298-7.

[17] Zhang C, Liu C, Zhao H, et al. Effect of nanoparticle and glass fiber on the hydrothermal aging of polyamide 6. Journal of Applied Polymer Science 2020; 137. DOI: 10.1002/app.49585.

[18] Sambale AK, Maisl M, Herrmann H-G, et al. Characterisation and Modelling of Moisture Gradients in Polyamide 6. Polymers 2021; 13. DOI: 10.3390/polym13183141.

[19] Dou Y, Mu X, Chen Y, et al. Effect of Composition on the Crystallization, Water Absorption, and Biodegradation of Poly(ε-caprolactam-co-ε-caprolactone) Copolymers. Polymers 2020; 12. DOI: 10.3390/polym12112488.

[20] Park M, Jang J-u, Park JH, et al. Enhanced Tensile Properties of Multi-Walled Carbon Nanotubes Filled Polyamide 6 Composites Based on Interface Modification and Reactive Extrusion. Polymers 2020; 12. DOI: 10.3390/polym12050997.

[21] Li Y, Nie D and Cai Z. The performance analysis of screw pump stator elastomers: Polyamide 6/hydrogenated nitrile blends: Mechanical, oil resistance and tribological properties. Polymer Testing 2023; 128. DOI: 10.1016/j.polymertesting.2023.108226.

[22] Heimrich M, Nickl H, Bönsch M, et al. Migration of Cyclic Monomer and Oligomers from Polyamide 6 and 66 Food Contact Materials into Food and Food Simulants: Direct Food Contact. Packaging Technology and Science 2015; 28: 123-139. DOI: 10.1002/pts.2094.

[23] Bomfim MVJ, Zamith HPS and Abrantes SMP. Migration of ε-caprolactam residues in packaging intended for contact with fatty foods. Food Control 2011; 22: 681-684. DOI: 10.1016/j.foodcont.2010.09.017.

[24] Sela R, Bychanok D, Padrez Y, et al. Electromagnetic properties of chloroprene rubber after long-term ultraviolet ageing, oil immersion and thermal degradation. Materials Research Express 2019; 6. DOI: 10.1088/2053-1591/ab1574.

[25] Bawase M, Chaudhari S and Thipse SS. Polymer/fuel interaction and properties of typical automotive fuel-system polymers exposed to methanol blended (M15) gasoline. Polymer Testing 2021; 97. DOI: 10.1016/j.polymertesting.2021.107141.

[26] Tormos B, Bermúdez V, Balaguer A, et al. Compatibility Study of Polyamide (PA6) with Lubricant Bases for Electric Vehicle Applications. Lubricants 2024; 12. DOI: 10.3390/lubricants12020054.

[27] He H, Wang X, Xu P, et al. Flower-like MnO2 nanoparticles modified thin film nanocomposite membranes for efficient organic solvent nanofiltration. Composites Communications 2023; 38. DOI: 10.1016/j.coco.2023.101515.

[28] Xu X, Shu X, Pei Q, et al. Effects of porosity on the tribological and mechanical properties of oil-impregnated polyimide. Tribology International 2022; 170. DOI: 10.1016/j.triboint.2022.107502.

[29] Kalácska G, Zsidai L, Keresztes R, et al. Effect of nitrogen plasma immersion ion implantation of polyamide-6 on its sliding properties against steel surface. Wear 2012; 290-291: 66-73. DOI: 10.1016/j.wear.2012.05.011.

[30] Durbin TD, Karavalakis G, Norbeck JM, et al. Material compatibility evaluation for elastomers, plastics, and metals exposed to ethanol and butanol blends. Fuel 2016; 163: 248-259. DOI: 10.1016/j.fuel.2015.09.060.